Journal of The
Electrochemical Society

Combining Molecular Dynamics and Experimental Methods for the Parametrization of Binary Carbonate-Based Electrolytes

To cite this article: Lukas Lehnert *et al* 2025 *J. Electrochem. Soc.* **172** 050523

Journal of The Electrochemical Society, 2025 **172** 050523

Combining Molecular Dynamics and Experimental Methods for the Parametrization of Binary Carbonate-Based Electrolytes

Lukas Lehnert,[1,2] Martin Lorenz,[3] Maria Fernanda Juarez,[1,2] Max Schammer,[1,2,4] Maryam Nojabaee,[5] Monika Schönhoff,[3] and Birger Horstmann[1,2,6,z]

[1]*German Aerospace Center, 89081 Ulm, Germany*
[2]*Helmholtz Institute Ulm, 89081 Ulm, Germany*
[3]*University of Münster, 48149 Münster, Germany*
[4]*Athene Patent, 81829 München, Germany*
[5]*German Aerospace Center, 70569 Stuttgart, Germany*
[6]*University of Ulm, 89081 Ulm, Germany*

Modelling the ionic transport in battery cells requires precise parametrization of the involved electrolytes. For carbonate-based electrolytes, however, the evaluation of their parameters suffers from interphase effects between the bulk electrolyte and the Li metal electrode, commonly present in the usual electrochemical polarization experiments. In this work, we combine measurements on conductivity and concentration cells with molecular dynamics simulations, avoiding these difficulties and thus, allowing for a more accurate determination of the parameters. We determine the conductivity, the transference number, the thermodynamic factor and the salt diffusion coefficient for three different electrolytes, i.e. mixtures of ethylene carbonate (EC), ethyl methyl carbonate (EMC), methyl propionate (MP), dimethyl carbonate (DMC) and propylene carbonate (PC), containing $LiPF_6$ at various concentrations and temperatures. In order to validate the simulated transference numbers, we employ electrophoretic Nuclear Magnetic Resonance spectroscopy (eNMR).

 [DOI: 10.1149/1945-7111/add381]

Manuscript submitted January 20, 2025; revised manuscript received March 31, 2025. Published May 19, 2025.

Supplementary material for this article is available online

The optimization of electrolytes plays a major role in developing Li^+ ion batteries. Adjusting the electrolyte composition allows for matching the transport properties to the battery operating conditions and can considerably improve the battery performance. This requires precise knowledge of the corresponding electrolyte parameters and thus calls for accurate characterization methods.

According to the concentrated solution theory from Latz's group,[1–3] binary electrolytes containing three components (e.g. cations, anions, solvent) comprise four independent parameters: the conductivity κ, a transference number t_α (where we choose the transference number of the Li^+ ions $\alpha = +$ for this paper), the thermodynamic factor *TDF*, and the salt diffusion coefficient $D_\pm$. While electrochemical impedance spectroscopy (EIS) of the electrolyte reveals κ, measurements on concentration cells determine convoluted information about t_+ and *TDF*.[4–7] Polarization experiments with symmetrical Li | electrolyte | Li cells enable the deconvolution of the data from the concentration cells and the measurement of the diffusion coefficient $D_\pm$. However and in contrast to the reproducible EIS and concentration cell techniques, the polarization experiments show inconsistent results for carbonate-based electrolytes.[4–6,8] As discussed in Refs. 6, 8, 9, interphasial effects between the Li metal electrodes and the electrolyte interfere with the experiments, hindering the evaluation of the polarization response.

Electrophoretic Nuclear Magnetic Resonance spectroscopy (eNMR) provides an experimental alternative to measuring t_+,[10–13] away from possible parasitic interphasial effects. In eNMR experiments, the electrolyte is exposed to an electric field, which induces a directed migration of the ionic species. The experiment measures the average drift velocity of each constituent in the bulk electrolyte and allows for an undisturbed, direct determination of t_+.[10–13]

Numerical methods like molecular dynamics (MD) simulations are completely unaffected by experimental difficulties.[14–19] MD simulations model the interactions between the atoms of a particle ensemble based on the underlying applied force fields. Calculating the corresponding individual trajectories provides deep insight into the temporal evolution of the examined system and its equilibrium fluctuations. According to the fluctuation-dissipation theorem,[20] the statistical behavior of these microscopic fluctuations determines the macroscopic thermodynamics of the particle ensemble and thus, reveals the desired electrolyte parameters.

Mistry et al. developed a set of non-linear algebraic equations, connecting the relative displacements of ions and solvent molecules to the Stefan-Maxwell diffusivities, which are directly related to the transport parameters of the corresponding electrolyte. This approach requires remarkably small trajectory information compared to similar methods to predict well-behaved trends with bounded variabilities.[19]

Fong et al. derived Green-Kubo relations, connecting correlations of particle flux fluctuations to the Onsager transport coefficients.[14,15] While this approach might not quite match the precision of Mistry et al., it still provides reasonably accurate transport coefficients within the given statistical error bars. Furthermore, the matrix of the Onsager transport coefficients is defined as positive semi-definite, a criterion which directly ensures positive entropy production and thus, thermodynamic consistency. Therefore, we follow the approach by Fong et al.

The combination of MD simulations and experimental data on concentration cells allows for a complete determination of the electrolyte parameters. Calculating the Onsager transport coefficients directly yields κ and t_+. The obtained transference number t_+ allows for deconvoluting the experimental concentration cell data, revealing the thermodynamic factor *TDF*. Specifying *TDF* finally enables the evaluation of the salt diffusion coefficient $D_\pm$.

The comparison of calculated conductivity values with experimental data allows for refining the MD simulations. Simulations using unpolarizable force fields often introduce an electrolyte specific scaling factor, which lowers the effective charges of the involved ions in order to compensate for the neglected screening effects due to solvent polarization.[16,21,22] Benchmarking the simulated conductivity results against experimental data enables identifying the scaling factor, and thus, yields more accurate simulation results.[23]

[z]E-mail: birger.horstmann@dlr.de

In this work, we determine the four electrolyte parameters of three systems, containing $LiPF_6$ in mixtures of ethylene carbonate (EC), ethyl methyl carbonate (EMC), methyl propionate (MP), dimethyl carbonate (DMC) and propylene carbonate (PC), at various concentrations ($0.1\,M \leqslant c \leqslant 3.0\,M$) and temperatures ($-20\,°C \leqslant T \leqslant 20\,°C$). The examined solutions are EC:EMC (3:7, weight), EC:DMC:PC (27:63:10, volume), and EC:EMC:MP (2:6:2, volume).

$LiPF_6$ in EC:EMC has already been examined many times, using electrochemical and numerical methods.[4–6,16,24] Thus, choosing this electrolyte for parametrization in our work allows for implementing experimental literature data in our characterization process, comparing the data to our results and benchmarking our numerical methods. $LiPF_6$ in EC:DMC:PC has also been experimentally characterized,[7] which likewise benefits our study. Additionally, although with unknown solvent mass or volume ratios, this electrolyte is employed in the commercial cell LG 18650 HG2.[25] The cell is currently under investigation in our group and thus, evaluating the parameters of the electrolyte in absence of possible, detrimental interphase effects between Li metal and the bulk electrolyte could therefore support future battery cycling simulations. The electrolyte $LiPF_6$ in EC:EMC:MP using $c = 1.0\,M$ has been developed by the Jet Propulsion Laboratory for the Mars InSight mission[26–28] and has space proven itself on the surface of Mars for several years. Therefore, this electrolyte poses an interesting candidate for its low temperature behavior.

For the determination of the electrolyte parameters, we combine EIS and measurements on concentration cells with MD simulations, using unpolarizable Optimized Potentials for Liquid Simulations (OPLS)[29] with an optimized scaling factor for the charges of the ions. In order to validate the modeled transference numbers, we conduct additional eNMR measurements of $LiPF_6$ in EC:EMC and in EC:EMC:MP at $0.5\,M \leqslant c \leqslant 1.5\,M$ and $T = 20\,°C$. Additionally, we investigate the simulated electrolyte viscosity using the Stokes-Einstein relation, the diffusion mechanism, and the formation of ion associations, and we estimate qualitatively their influence on the transport parameters.

The subsequent section gives a brief overview of the theory governing the equations of the MD simulations, the EIS, the concentration cells, and the eNMR measurements. This section is followed by the evaluation of the electrolyte parameters and their fitting functions. The final section estimates the dependence of the transport parameters on the additionally calculated electrolyte characteristics mentioned above.

Theory

Molecular Dynamics (MD).—We calculate the transport parameters for $LiPF_6$ in EC:EMC, in EC:DMC:PC and in EC:EMC:MP using MD simulations. For this, we summarize the essential equations in this section, following the theoretical framework derived by Fong et al. A detailed derivation is given in Refs. 14, 15, 30.

Fong et al. base their theory on the Onsager transport equations

$$\boldsymbol{J_i} = -\sum_j L^{ij} \nabla \mu_j, \qquad [1]$$

where $\boldsymbol{J_i}$ denotes the particle flux of species i relative to the center-of-mass velocity and μ_j is the electrochemical potential of species j. The flux and the driving forces are linearly coupled via the Onsager transport coefficients L^{ij}. These coefficients are later translated into the transport parameters of the electrolyte (see Eqs. 4–6).

In order to calculate L^{ij}, Fong et al. derive Green-Kubo relations connecting the Onsager coefficients to a correlation function between the fluxes $\boldsymbol{J_i}$ and $\boldsymbol{J_j}$,

$$L^{ij} = \frac{V}{3k_B T} \int_0^\infty \mathrm{d}t \, \langle \boldsymbol{J_i}(t) \cdot \boldsymbol{J_j}(0) \rangle \qquad [2]$$

with the ensemble volume V, the Boltzmann constant k_B, and the temperature T. Notably, this equation suggests interpreting L^{ij} as a degree of motion correlation between the species i and j.[15] The equation can be also reformulated into an expression depending on the individual particle positions $\boldsymbol{r}_i^\alpha$ and $\boldsymbol{r}_j^\beta$ with respect to the position of the center-of-mass,[15]

$$L^{ij} = \frac{1}{6k_B TV} \lim_{t\to\infty} \frac{\mathrm{d}}{\mathrm{d}t} \left\langle \sum_\alpha [\boldsymbol{r}_i^\alpha(t) - \boldsymbol{r}_i^\alpha(0)] \cdot \sum_\beta [\boldsymbol{r}_j^\beta(t) - \boldsymbol{r}_j^\beta(0)] \right\rangle. \qquad [3]$$

Here, we use Eq. 3 to determine the coefficients L^{ij} for binary electrolytes with three components: Li^+, and PF_6^- ions, and solvent molecules. The number of the corresponding independent Onsager transport coefficients reduces to $n(n-1)/2 = 3$ (where n is the number of components), due to the Onsager reciprocal relations $L^{ij} = L^{ji}$.[31,32] Therefore, we evaluate the particle trajectories of the ions to calculate L^{++}, L^{--} and L^{+-}. Note that this merging of multiple solvent species into one single "pseudo" solvent simplifies the underlying transport mechanisms. As previous research shows, the components of a solvent mixture exhibit their individual mobilities, contributing to the transport phenomena in the corresponding electrolyte.[33–37] Thus, a complete and detailed description of the transport properties would require the determination of an increased number of Onsager transport coefficients, accounting for these mobilities. However, we believe that an accurate electrochemical battery model can still be achieved even using a simplified model with lower computational complexity. The advantages of using these valid simplifications relies on the possibility of describing the internal electrochemical mechanism of batteries with higher precision. In these cases, other advanced techniques, like machine learning or quantum computing algorithms, can be applied to improve the accuracy of the models. The use of these new technologies also allows for increasing the complexity of the initial models, as the stacking technique can be used in these algorithms.

The Onsager transport coefficients are translated into the transport parameters of the electrolyte. For our binary systems (with the stoichiometric factors $\nu_+ = \nu_- = 1$) the conductivity κ, the transference number t_+ and the salt diffusion coefficient $D_\pm$ read[14,15,30]

$$\kappa = F^2(z_+^2 L^{++} + 2z_+z_-L^{+-} + z_-^2 L^{--}), \qquad [4]$$

$$t_+ = \frac{z_+^2 L^{++} + z_+z_-L^{+-}}{z_+^2 L^{++} + 2z_+z_-L^{+-} + z_-^2 L^{--}}, \qquad [5]$$

$$D_\pm = \frac{-z_+z_-(L^{++}L^{--} - L^{+-2})}{z_+^2 L^{++} + 2z_+z_-L^{+-} + z_-^2 L^{--}} \frac{RT}{c} TDF \qquad [6]$$

with the charge numbers $z_+ = 1$ and $z_- = -1$ of the ions, the Faraday constant F, and the ideal gas constant R. The thermodynamic factor $TDF = 1 + \frac{\mathrm{d}\ln f_\pm}{\mathrm{d}\ln c}$ comprises the salt activity coefficient $f_\pm$ and is generally unknown. In order to reveal TDF, the authors combine the MD simulations with concentration cell measurements, yielding a convoluted expression of t_+ and TDF as a function of c and T (see Eqs. 11–14 in the subsequent section). The combination allows for deconvoluting the thermodynamic factor TDF and hence enables the calculation of $D_\pm$, completing the determination of the four electrolyte parameters. Alternatively, although not done in this work, the TDF can be directly calculated from MD simulations using numerical methods such as thermodynamic integration, Kirkwood-Buff integrals or the S0 method.[38–42] Note that Fong et al. define TDF using the chemical

potential of the Li^+ ions.[43] Instead, we use the chemical potential of the neutral salt summing up the chemical potential of anions and cations, weighted with the correct stoichiometric factors.[1,2] Therefore, Eq. 6 deviates by a factor $\frac{1}{2}$ from the relation in Ref. 14. Technical details on the employed simulations and the computational methods can be found in the supplementary information (see SI Section S1.1–S1.4).[4,7,15,16,21,29,44–62]

Considering our transport theory, the fluxes of the individual species are defined with respect to some reference velocity $\boldsymbol{v}^{\Psi}$.[63] The choice of the reference frame Ψ directly affects the effective electrochemical potential of the electrolyte μ^{Ψ} and the Onsager transport coefficients $L^{ij,\Psi}$. Therefore, MD simulations and experiments conducted in different reference frames yield deviating electrolyte parameters. A direct comparison of the parameters thus requires a transformation into the same reference frame.

In MD, the calculation of the transport parameters (see Eqs. 4–6) often uses the velocity of the center-of-mass (COM) as reference frame.[16] In contrast, some other groups have shown that eNMR measurements capture the transference number t_+ in a reference frame with local volume conservation (VOL).[64,65] In order to compare the MD simulations to the eNMR experiments, we transform the calculated parameters from the COM into the VOL reference frame (see SI Eqs. S6–S8).[63,66,67] For our locally electro-neutral electrolytes, the transformations read

$$\kappa^{\mathrm{VOL}} = \kappa^{\mathrm{COM}}, \tag{7}$$

$$t_+^{\mathrm{VOL}} = \frac{c_0\nu_0}{\omega_0}(t_+^{\mathrm{COM}} - \omega_-) + c_-\nu_-, \tag{8}$$

$$\frac{D_\pm^{\mathrm{VOL}}}{TDF^{\mathrm{VOL}}} = \frac{c_0^2\nu_0^2}{\omega_0^2}\frac{D_\pm^{\mathrm{COM}}}{TDF^{\mathrm{COM}}} \tag{9}$$

with the partial molar volume ν_i and the mass fraction ω_i of species i. Based on the findings of Lorenz[64] and Kilchert,[65] we expect that the concentration cells capture information about the transference number t_+ and the thermodynamic factor TDF in the volume-based frame (see Eqs. 11–14).

While we focus on the volume-based frame in this work, the literature often presents the electrolyte parameters in different reference frames. Therefore, we additionally present our findings in the COM and in the solvent-velocity reference frame (SOL) in the supplementary information (see SI Figs. S3, S4 and SI Tables S5, S6).

Experimental.— *Conductivity cell.*—Experimental conductivity data enable benchmarking and improving the MD simulations by adjusting the scaling factor for the effective charges of the involved ions. Performing EIS reveals the bulk resistance R_{el} of the electrolyte, which translates to the corresponding conductivity κ with[4–7]

$$\kappa = \frac{k}{R_{\mathrm{el}}}. \tag{10}$$

The cell constant k captures the geometrical characteristics of the conductivity cell and can be measured by using a reference electrolyte with known conductivity. Experimental details can be found in the supplementary information (see SI Section S2.1).

Concentration cell.—Concentration cells comprise two identical electrodes (in our case Li metal electrodes), immersed in separated electrolyte solutions with slightly different concentrations c_{L} and c_{R}. A salt bridge ionically connects the two solutions, enabling a finite but negligibly small current to flow. This allows for measuring the concentration potential U_{c} between the electrodes. Considering the theory of concentrated electrolytes introduced by Latz et al.,[1,2] U_{c} includes convoluted information about the transference number t_+ and the thermodynamic factor TDF in form of $a(c, T) = (1 - t_+)TDF$,

$$U_{\mathrm{c}} = \frac{RT}{F}\int_{c_{\mathrm{L}}}^{c_{\mathrm{R}}} a(c, T)\, d\ln c. \tag{11}$$

Following the approach of Valøen et al.,[7] $a(c, T)$ can be expressed by a Taylor expansion,

$$\begin{aligned} a(c, T) &= a_0(T) + a_1(T)c^{1/2} + a_2(T)c^1 + \cdots \\ &= \sum_{i=0}^{n} a_i(T)c^{i/2}, \end{aligned} \tag{12}$$

where the coefficients $a_i(T) = a_{i0}[1 + a_{i1}(T - T_0)]$ depend linearly on the temperature with $T_0 = 293.15$ K. The insertion of Eq. 12 into Eq. 11 and subsequent integration relates the potential U_{c} directly to the coefficients $a_i(T)$,[7]

$$\frac{F}{RT}U_{\mathrm{c}} = a_0(T)[\ln c]_{c_{\mathrm{L}}}^{c_{\mathrm{R}}} + \sum_{i=1}^{n} a_i(T)\frac{2}{i}[c^{i/2}]_{c_{\mathrm{L}}}^{c_{\mathrm{R}}}. \tag{13}$$

Therefore, the measurement of multiple concentration cells at different temperatures T and concentration pairs c_{L} and c_{R} allows for determining the coefficients $a_i(T)$ and thus, reveals $a(c, T)$. As mentioned above, the expressions for U_{c} derived in Eqs. 11 and 13 using our theory differ by a factor of 2 from similar expressions using the concentrated solution theory by Newman.[43]

Combining the results of the MD simulations for t_+ (see Eq. 5) with $a(c, T)$ deconvolutes the thermodynamic factor,

$$TDF = \frac{a(c, T)}{1 - t_+}. \tag{14}$$

As mentioned above, we use the measurements on concentration cells to determine $a^{\mathrm{VOL}}(c, T)$ in the VOL reference frame. For the sake of comparison and completeness, the deconvolution of TDF^{VOL} has therefore to be done with t_+^{VOL}. Experimental details can be found in the supplementary information (see SI Sections S2.1 and S2.2).

eNMR.—Electrophoretic Nuclear Magnetic Resonance (eNMR) allows for the determination of ion-specific drift velocities v in an applied electric field $E = \frac{U}{d}$. Here, U denotes the voltage between the two electrodes and d the electrode distance. In contrast to random diffusive motion, which leads to a decay of the measured NMR echo intensity in an echo experiment with pulsed magnetic field gradients, the coherent migrational flux of ions causes a phase shift of the NMR-signal. This can be read out using phase sensitive Lorentzian-type fit functions as previously described.[68] The obtained phase shift $\phi - \phi_0$ is then connected with the electrophoretic mobility $u = \frac{v}{E}$ of the respective ionic constituent according to[69]

$$\phi - \phi_0 = \delta\Delta\gamma g E u \tag{15}$$

with the observation time Δ, the gradient pulse duration δ, the gyromagnetic ratio γ, and the gradient strength g. Consequently, u can be determined from a linear fit of $\phi - \phi_0$ against U (see SI Fig. S27). The obtained electrophoretic mobilities u_+ and u_- for the Li^+ and PF_6^- ions translate to the transference number t_+ according to

$$t_+ = \frac{z_+u_+}{z_+u_+ + z_-u_-}. \tag{16}$$

As mentioned above, the eNMR measurements capture the electrophoretic mobilities and transference numbers in the VOL reference frame. Experimental details can be found in the supplementary information (see SI Sections S2.1 and S2.3).[12,70]

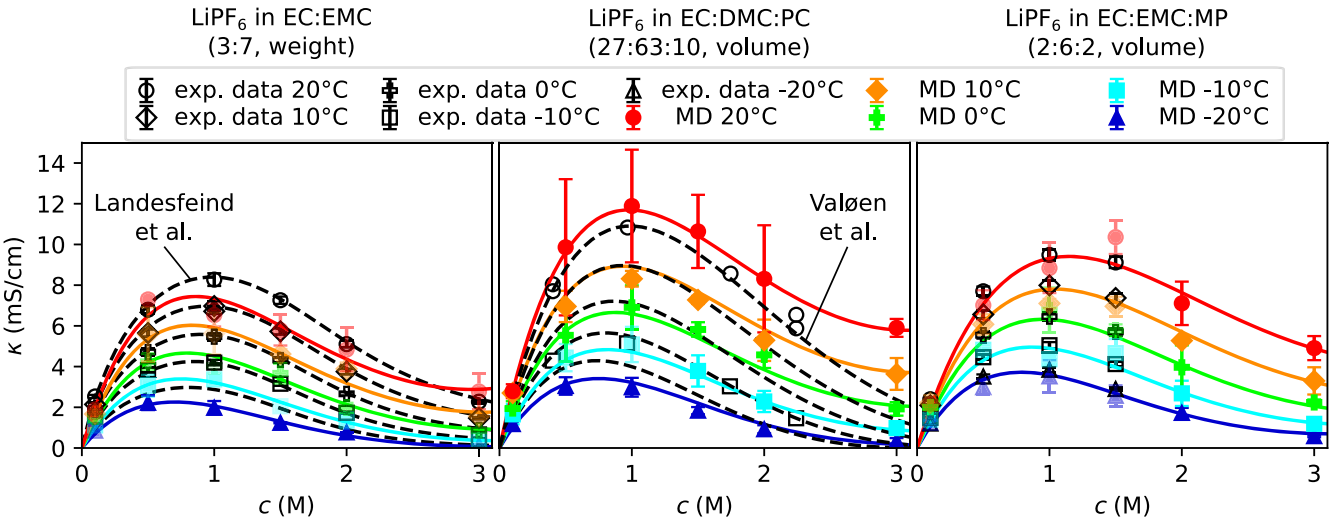

Figure 1. Conductivities κ obtained by MD simulations and electrochemical measurements, together with their corresponding fit functions (solid and dashed lines). The experimental conductivities for $LiPF_6$ in EC:EMC and in EC:DMC:PC were taken from Landesfeind et al.[4] and Valøen et al.[7]

Results

This section presents the evaluation of the electrolyte parameters in the VOL reference frame for our three electrolytes at various concentrations and temperatures. The transformed parameters in the COM and SOL frame can be found in the supplementary information (see SI Figs. S3, S4 and SI Tables S5, S6). While these parameter-sets are obtained using the method of Fong et al.[14,15], we additionally apply the method of Misty et al.[19] exemplary for one electrolyte in the supplementary information (see SI Fig. S7). Note that capturing crystal nucleation in liquids is challenging for MD simulations.[71] Therefore, the simulations do not predict any possible phase transitions and thus, the parameters at low temperatures have to be treated with care.

Conductivity.—Figure 1 shows the conductivity results κ of the MD simulations for our three electrolytes together with the corresponding experimental data.[4,7] In general, the simulations match the experimental values well and exhibit for each electrolyte a similar trend: κ increases with concentration up to a maximum, before it declines to lower values. Elevating the temperature enhances the conductivity.

The accordance to the experimental data indicates that the MD simulations capture the behavior of the electrolytes reasonably well for concentrations below $c = 2.0\,\mathrm{M}$. However, the MD simulations overestimate the conductivity for $LiPF_6$ in EC:EMC and in EC:DMC:PC at $c = 3.0\,\mathrm{M}$. This could originate from using a constant scaling factor ζ, omitting any concentration dependence of the solvent screening effects due to solvent polarization. At elevated concentrations, the ratio of ions to solvent molecules increases drastically, minimizing the number of solvent molecules in the first solvation shell (see SI Figs. S10, S11) and the corresponding solvent screening effects. Therefore, employing a constant scaling factor might underestimate the effective ionic charges at $c = 3.0\,\mathrm{M}$, resulting in an underestimated number of ion associations and thus, yielding elevated conductivities in the MD simulations. Note that the deviation in conductivity might hint to similar deviations, occurring in other electrolyte parameters at elevated concentrations.

Using the functional form proposed by Valøen et al.[7], we fit the simulated conductivities κ with Eq. 17. Table I shows the corresponding coefficients κ_{ij} for our three electrolytes.

$$\sqrt{\frac{\kappa}{c}} = \sum_{i=0}^{n} \sum_{j=0}^{k} \kappa_{ij} c^i T^j \qquad [17]$$

Table I. Fit coefficients κ_{ij} (in $(\mathrm{mS/cm})^{0.5}\,\mathrm{M}^{-i-0.5}\,\mathrm{K}^{-j}$) for the conductivities κ.

Parameter	$LiPF_6$ in EC: EMC (3:7, weight)	$LiPF_6$ in EC: DMC:PC (27:63:10, volume)	$LiPF_6$ in EC: EMC:MP (2:6:2, volume)
κ_{00}	$-2.438 \cdot 10^{1}$	$1.876 \cdot 10^{0}$	$-1.992 \cdot 10^{1}$
κ_{01}	$1.597 \cdot 10^{-1}$	$-3.655 \cdot 10^{-2}$	$1.471 \cdot 10^{-1}$
κ_{02}	$-2.067 \cdot 10^{-4}$	$1.673 \cdot 10^{-4}$	$-2.168 \cdot 10^{-4}$
κ_{10}	$8.677 \cdot 10^{0}$	$-2.592 \cdot 10^{0}$	$6.400 \cdot 10^{0}$
κ_{11}	$-6.024 \cdot 10^{-2}$	$2.035 \cdot 10^{-2}$	$-6.206 \cdot 10^{-2}$
κ_{12}	$7.730 \cdot 10^{-5}$	$-6.821 \cdot 10^{-5}$	$1.171 \cdot 10^{-4}$
κ_{20}	$-5.380 \cdot 10^{-1}$	$-4.285 \cdot 10^{-1}$	$6.877 \cdot 10^{-1}$
κ_{21}	$3.093 \cdot 10^{-3}$	$2.717 \cdot 10^{-3}$	$-1.628 \cdot 10^{-3}$

Transference number.—The MD simulations yield similar low transference numbers t_+^{VOL} for our three electrolytes (see Fig. 2), indicating that primarily the PF_6^- ions contribute to the ionic conductivity. This matches fairly well with the experimental results of Valøen et al.[7] for $LiPF_6$ in EC:DMC:PC and the eNMR measurements at 20 °C for $LiPF_6$ in EC:EMC and EC:EMC:MP. However, our findings deviate from the galvanostatic polarization data from Landesfeind et al.[4] for $LiPF_6$ in EC:EMC. In their work, they find that t_+^{VOL} correlates with both concentration and temperature, yielding even negative transference numbers at low temperatures. In contrast, our MD simulations do not resolve any visible dependence of t_+^{VOL} on the concentration or the temperature, which is consistent with the MD simulation results from Ringsby et al.[16] at $c = 1.0\,\mathrm{M}$. The discrepancy probably originates from the difficulty of determining the transport parameters of carbonate-based electrolytes using polarization experiments with Li metal electrodes. In these experiments, porous, mossy Li and solid-electrolyte interphase (SEI) layers cover the initially pristine Li metal electrode, influencing the induced concentration gradient and thus, the potential response.[6,8,9] The MD simulations as well as the eNMR measurements do not suffer from these surface effects and can therefore provide more precise values for the transference numbers t_+^{VOL}. Hence, the accordance of the calculated MD data with the eNMR results validates the integrity of our simulations.

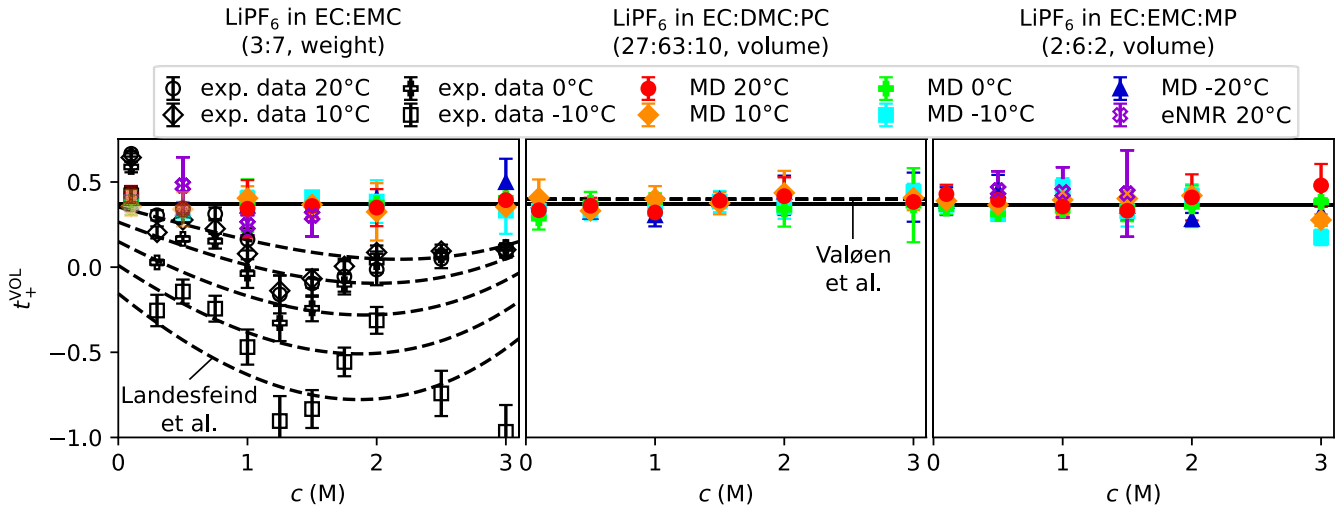

Figure 2. Transference numbers t_+^{VOL} in the VOL reference frame obtained by MD simulations, electrochemical experiments and eNMR measurements, together with their corresponding fit functions (solid and dashed lines). The transference numbers of $LiPF_6$ in EC:EMC and in EC:DMC:PC were taken from Landesfeind et al.[4] and Valøen et al.[7]

Table II. Constant fit coefficients for the transference numbers t_+^{VOL} from our MD simulations, compared to our eNMR measurements and the findings of Valøen et al.[7]

Parameter	$LiPF_6$ in EC:EMC (3:7, weight)	$LiPF_6$ in EC:DMC:PC (27:63:10, volume)	$LiPF_6$ in EC:EMC:MP (2:6:2, volume)
t_+^{VOL} (MD)	0.373	0.372	0.366
t_+^{VOL} (eNMR)	0.343	—	0.441
t_+^{VOL} (Valøen et al.[7])	—	0.399	—

Since t_+^{VOL} lacks any visible trend in our MD simulations due to the scattering of the data, we fit the data with a constant. Table II lists the corresponding values.

Thermodynamic factor.—The experiments on concentration cells allow for the determination of $a^{VOL}(c, T) = (1 - t_+^{VOL})TDF^{VOL}$, containing convoluted information about the transference number and the thermodynamic factor (see Eqs. 11–13). Hence, the combination of the MD simulations determining t_+^{VOL} and the measurements on concentration cells reveals the thermodynamic factor TDF^{VOL} (see Eq. 14).

Valøen et al.[7] conduct experiments on concentration cells for $LiPF_6$ in EC:DMC:PC and fit the determined potentials with Eq. 13 to obtain $a^{VOL}(c, T)$. In the fitting process, the authors set $a_2 = 0$ and introduce the temperature dependence solely in $a_3(T)$ while keeping a_0 and a_1 constant (i.e. $a_{01} = a_{11} = 0$). This results in a total of four fitting coefficients a_{00}, a_{10}, a_{30} and a_{31}.

In order to find $a^{VOL}(c, T)$ for $LiPF_6$ in EC:EMC and $LiPF_6$ in EC:EMC:MP, we apply the same procedure to the data provided by Landesfeind et al.[4] and our own concentration cell data (see SI Fig. S23). Table III lists the corresponding coefficients $a_i(T)$.

Inserting the obtained fit function $a^{VOL}(c, T)$ together with our MD simulation results for t_+^{VOL} in Eq. 14 determines the thermodynamic factor TDF^{VOL} (see Fig. 3). TDF^{VOL} exhibits for all three electrolytes a similar shape with increasing values with increasing concentration and decreasing temperature. While our simulated data match well with the experimental findings of Valøen et al. for $LiPF_6$ in EC:DMC:PC, they deviate from the results from Landesfeind et al. for $LiPF_6$ in EC:EMC. The reason for this discrepancy probably arises from the challenging determination of t_+^{VOL} using Li metal electrodes together with carbonate-based electrolytes in polarization experiments, as mentioned above.[8]

Note that TDF^{VOL} in our theory[3] differs from TDF^{VOL} derived by Newman's concentrated solution theory[43] by a factor of 2, as mentioned above. In order to compare with our set of fit parameters, we multiplied the literature data in Fig. 3 by this factor.

Also note that concentration cells at very low temperatures show irregular ice formation for identical cells, revealing the electrolyte as a supercooled fluid (see SI Figs. S24–S26).

Diffusion coefficient.—The salt diffusion coefficient $D_\pm^{VOL}$ obtained by our MD simulations shows a clear deviation from the results of the electrochemical experiments (see Fig. 4).[4,7] Even though the increasing trend with temperature coincides, the concentration dependence differs and rather resembles the findings of Logan et al.[72], using the Advanced Electrolyte Model[73,74] to calculate the salt diffusion coefficient for $LiPF_6$ in EC:DMC (3:7, weight) at 20 °C. While our calculations exhibit a more complex shape with elevated $D_\pm^{VOL}$ even at higher concentrations, the experiments find monotonously decreasing values with increasing concentration. As mentioned above, this deviation could originate from additional porous layers of mossy Li and SEI, influencing the potential response in the galvanostatic polarization experiments and hence, making the electrochemical determination of the diffusion coefficient $D_\pm^{VOL}$ difficult. We further analyze the diffusion coefficient trends in the SI (see SI Section S1.6), using $LiPF_6$ in EC:EMC as an example, and compare them to the diffusion coefficient trends of the solid polymer electrolyte lithium bis(trifluoromethanesulfonyl)imide (LiTFSI) in poly(ethylene oxide) (PEO).[75] The polymer electrolyte does not suffer from detrimental effects in the polarization measurements and thus, should yield more trustworthy experimental data of the diffusion coefficient than carbonate-based electrolytes.

In order to represent the MD data in an analytic form, we take the same approach as Valøen et al.[7] and fit the data to an exponential function

$$\log_{10} D_\pm^{VOL} = \sum_{i=0}^{n} D_i(c, T)c^i, \qquad [18]$$

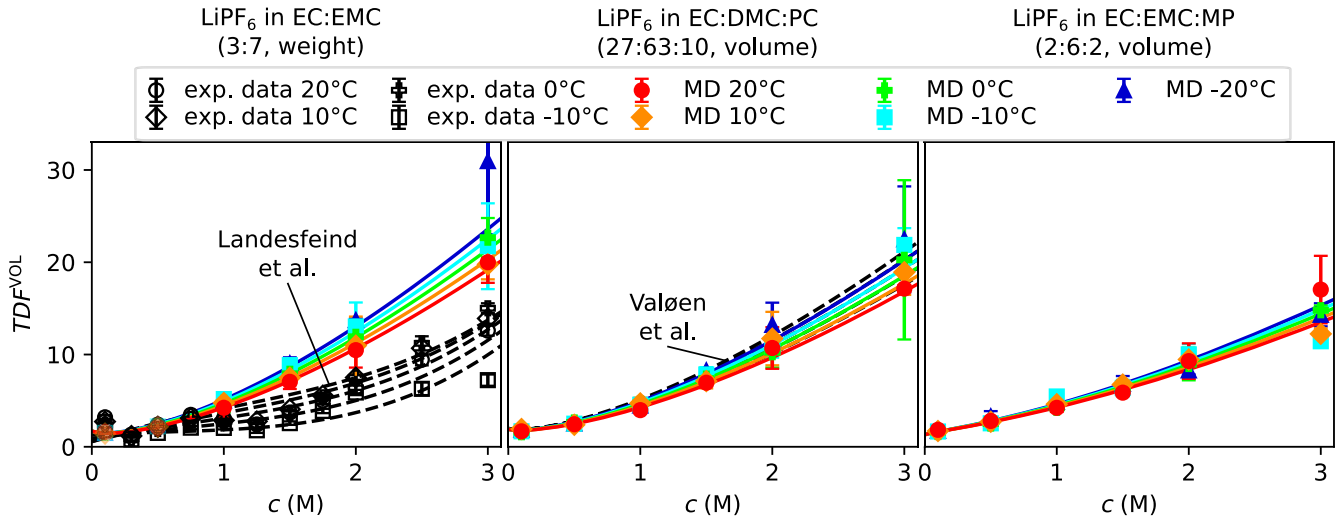

Figure 3. Thermodynamic factors TDF^{VOL} in the VOL reference frame determined by combining concentration cell measurements with MD simulations or polarization experiments.[4,7] The solid and dashed lines show their corresponding fit functions. Note that we multiply the literature data by a factor of 2, as mentioned in the main text.

Table III. Fit coefficients T_0 (in K) and a_{ij} (in $\mathrm{M}^{-\delta_{ij}i/2}\,\mathrm{K}^{-j}$) for $a^{\mathrm{VOL}}(c, T)$.

Parameter	$LiPF_6$ in EC:EMC (3:7, weight)	$LiPF_6$ in EC:DMC:PC (27:63:10, volume)	$LiPF_6$ in EC:EMC:MP (2:6:2, volume)
T_0	293.15	293.15[a)]	293.15
a_{00}	$1.085 \cdot 10^{0}$	$1.202 \cdot 10^{0}$[a)]	$8.134 \cdot 10^{-1}$
a_{10}	$-7.761 \cdot 10^{-1}$	$-4.800 \cdot 10^{-1}$[a)]	$5.980 \cdot 10^{-1}$
a_{30}	$2.365 \cdot 10^{0}$	$1.964 \cdot 10^{0}$[a)]	$1.291 \cdot 10^{0}$
a_{31}	$-5.627 \cdot 10^{-3}$	$-5.200 \cdot 10^{-3}$[a)]	$-4.308 \cdot 10^{-3}$

a) Adapted from Valøen et al.[7]

where

$$D_i(c, T) = \sum_{j=0}^{n} \frac{D_{ij}}{[T - (T_{g0} + cT_{g1})]^j}. \qquad [19]$$

Table IV shows the corresponding coefficients T_{gi} and D_{ij} for our three electrolytes.

Discussion

Ionic transport in concentrated electrolytes is a complex phenomenon. In order to precisely predict the electrolyte characteristics, a multitude of interactions have to be considered in detail.[74] In this section, we roughly analyze the trends of the solvation shell size, the viscosity, the diffusion mechanisms, and the number of ion associations for our three electrolytes and qualitatively estimate their impacts on the ionic transport. For simplicity, we approximate and analyze the transport parameters using dilute solution theory in the COM frame. Computational details and further analysis of the radial distribution function (RDF), the coordination numbers of the ions, the viscosity, the residence time, the diffusion length, the ion association and the ionic mobility can be found in the supplementary information (see SI Section S1.8–S1.12).[15–17,24,73,74,76–99]

Solvation shell radius and electrolyte viscosity.—The radius of the ion solvation shell r_s and the electrolyte viscosity η directly impact the ionic transport. Assuming Stoke's Law as an approximation for our concentrated electrolytes,[100] the dragging force on a solvated ion is directly proportional to both r_s and η. According to this equation, large solvation shell radii and more viscous electrolytes lead to slower movement and lower mobilities of the ions (see SI Section S1.12).

While in our MD simulations the composition of the ion solvation shells changes, the corresponding size is independent from temperature and concentration and is similar for our three electrolytes (see SI Fig. S9). Consequently, we assume that the solvation shell radius does not contribute to any differences in the transport parameters of our three electrolytes.

The viscosity η can be approximated using the Stokes-Einstein relation, which connects the diffusion of spherical particles through a liquid to the liquid's viscosity

$$\eta = \frac{k_B T}{6\pi D_{\mathrm{self}}^{\mathrm{COM}} r(c)}, \qquad [20]$$

where $D_{\mathrm{self}}^{\mathrm{COM}}$ denotes the self-diffusion coefficient in the COM frame and $r(c)$ the radius of the particles. To apply the Stokes-Einstein relation in our work, we approximate the three component mixture of our electrolytes as a single component liquid, consisting of identical, spherical particles. The corresponding effective self-diffusion coefficient $D_{\mathrm{self}}^{\mathrm{COM}}$ of the spherical particles is calculated by composition-weighted averaging the self-diffusion coefficients $D_{\mathrm{self}}^{i,\mathrm{COM}}$ of the individual electrolyte species i

$$D_{\mathrm{self}}^{\mathrm{COM}} = \sum_{i}^{n} \omega_i D_{\mathrm{self}}^{i,\mathrm{COM}}, \qquad [21]$$

where ω_i denotes the species mass ratio (see SI Eqs. S19–S21). Additionally, we compare our calculated viscosity values to experimental data to estimate the effective particle radius $r(c)$ (see SI Fig. S13). In contrast to the solvation shell radius r_s of the ions, $r(c)$ represents the average size of all particles involved, including the solvent molecules. Note that Ringsby et al. consider only the self-diffusion coefficients of the solvent species to separate the influence of solvent viscosity and ion association on the transport parameters.[16] For our electrolytes, however, the electrolyte viscosity and the solvent viscosity are almost identical (see SI Fig. S15). Therefore, and for the sake of simplicity, we incorporate the self-diffusion coefficients of all species in our calculations. Alternatively, although not done here, the viscosity can also be determined directly from MD simulations using the Green-Kubo relation or inferred from finite size effects.[101–103]

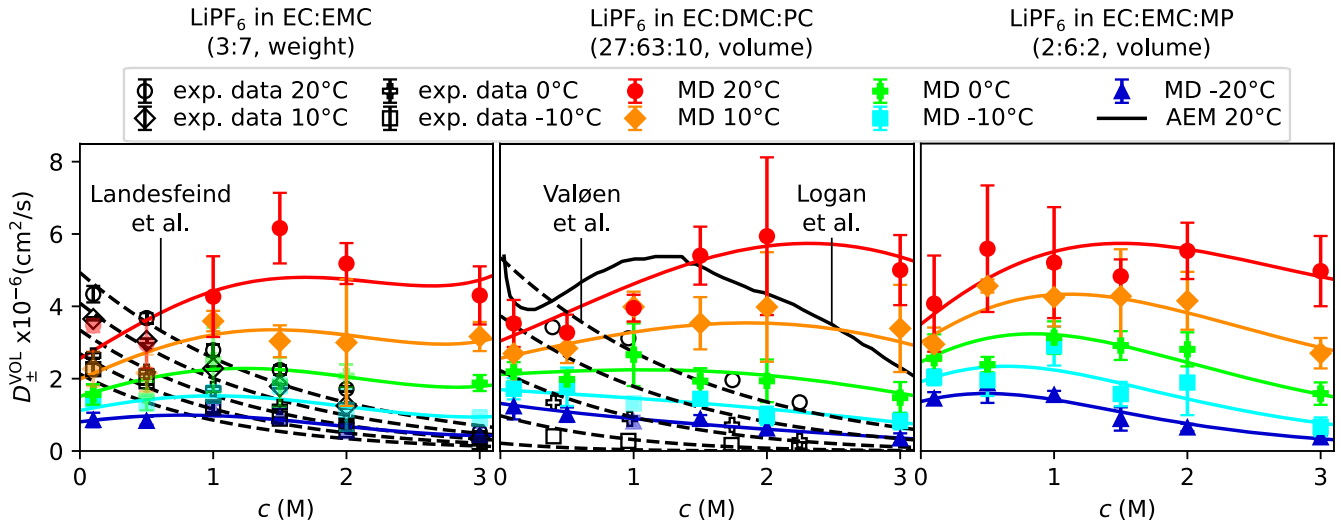

Figure 4. Diffusion coefficients $D_{\pm}^{\mathrm{VOL}}$ in the VOL reference frame calculated with MD simulations, the Advanced Electrolyte Model (AEM)[72–74] or electrochemically measured[4,7] together with their corresponding fit functions. Note that the AEM calculations determine the diffusion coefficient of a similar electrolyte $LiPF_6$ in EC:DMC (3:7, weight) over molal concentrations, slightly deviating from molar concentrations (see SI Fig. S14).

Table IV. Fit coefficients T_{gi} (in K M^{-i}) and D_{ij} (in K^j M^{-i}) for the diffusion coefficients $D_{\pm}^{\mathrm{VOL}}$.

Parameter	$LiPF_6$ in EC: EMC (3:7, weight)	$LiPF_6$ in EC: DMC:PC (27:63:10, volume)	$LiPF_6$ in EC: EMC:MP (2:6:2, volume)
T_{g0}	$4.988 \cdot 10^{1}$	$1.209 \cdot 10^{2}$	$1.929 \cdot 10^{2}$
T_{g1}	$3.945 \cdot 10^{1}$	$-1.363 \cdot 10^{1}$	$-1.649 \cdot 10^{1}$
D_{00}	$-3.047 \cdot 10^{0}$	$-4.313 \cdot 10^{0}$	$-4.840 \cdot 10^{0}$
D_{01}	$-6.191 \cdot 10^{2}$	$-2.074 \cdot 10^{2}$	$-6.168 \cdot 10^{1}$
D_{10}	$5.685 \cdot 10^{-1}$	$1.676 \cdot 10^{0}$	$6.214 \cdot 10^{-1}$
D_{11}	$5.253 \cdot 10^{1}$	$-2.676 \cdot 10^{2}$	$-3.685 \cdot 10^{1}$
D_{20}	$-1.962 \cdot 10^{-1}$	$-1.000 \cdot 10^{-1}$	$9.174 \cdot 10^{-2}$
D_{21}	$2.050 \cdot 10^{1}$	$-8.239 \cdot 10^{0}$	$-3.354 \cdot 10^{1}$

Figure 5 shows the approximated viscosity η for all three electrolytes. Our calculated data match the Arrhenius fit of the experimental data η_{exp} for $LiPF_6$ in EC:EMC (see SI Eq. S22 and SI Table S8) and exhibit for all three electrolytes similar trends: η increases with concentration and decreases with temperature. Therefore, the particles experience less drag and enhanced mobility at low concentrations and high temperatures. Overall, $LiPF_6$ in EC:EMC reveals the highest and $LiPF_6$ in EC:EMC:MP the lowest viscosity, suggesting an increasing particle mobility in the same order.

Diffusion mechanism.—The interaction between the solvent molecules and ions dictates the diffusion mechanism of the ions. Vehicular type diffusion describes the motion of ions surrounded by a stable solvation shell. The individual solvent molecules of species i within the solvation shell accompany the ions over long diffusion lengths L_i before they are substituted by other molecules or ions. In contrast, structural type diffusion reveals short L_i, resulting in an ion hopping process with a rapid exchange of solvation shell molecules.[16,78,89] This type of diffusion relates to faster movement speeds of the ions.[16,74,91,92]

In order to estimate which diffusion mechanism is prevalent in our three electrolytes, we calculate the corresponding composition-weighted diffusion lengths $L = \sum_i^n \omega_i L_i$ (for L_i, see SI Figs. S19, S20) of the solvent molecules surrounding the Li^+ and the PF_6^- ions. L shows for all electrolytes similar results (see Fig. 6). While the solvent molecules of the Li^+ ion solvation shell exhibit decreasing diffusion lengths with concentration and temperature, the molecules surrounding the PF_6^- ion reveal fairly constant and overall lower values for L. This indicates that the solvent molecules are more strongly bound to the Li^+ ion,[84] even at the highest temperatures and concentrations. Consequently, the Li^+ ions exhibit a more vehicular type of transport than the PF_6^- ions.

Note that the diffusion mechanism can also be analyzed using different methods, as for instance shown in Refs. 19, 104.

Ion association.—Ion associations are defined by the particles occupying the solvation shell. An ion association is formed, if at least one additional ion populates the same solvation shell. This reduces the number of free ions (FI) in the electrolyte, influencing the transport properties of the electrolyte. Additionally, the formation of charged associations, like negative or positive triple ions (NTI, PTI) can cause the involved Li^+ and PF_6^- ions to migrate contrary to the expected direction. This was experimentally demonstrated at very high ion concentrations, namely for Li^+ ions in an ionic-liquid-based electrolyte.[10,11]

In order to calculate the number of free Li^+ and PF_6^- ions, we analyze the population of the corresponding solvation shells (see SI Fig. S21). Figure 7 shows that both ion species exhibit for all three electrolytes similar behavior: the fraction of FI decreases with temperature and concentration. This leads to a bell shaped behavior of the total FI concentrations, where the highest values are observed at low temperatures and intermediate salt concentrations. At elevated salt concentrations, the number of FI is slightly lower for the PF_6^- ions compared to the Li^+ ions. Our obtained FI concentrations for 1 M $LiPF_6$ in EC:EMC match the data from Ringsby et al.,[16] using a scaling factor of $\zeta = 0.8$ in their MD simulations. Further analysis of the data can be found in the supplementary information (see SI Section S1.11).

Overall, $LiPF_6$ in EC:DMC:PC exhibits the highest FI concentrations. This could be due to its elevated cyclic carbonate concentration (see SI Table S1), as cyclic carbonates improve the solubility of the ions.[85] $LiPF_6$ in EC:EMC and $LiPF_6$ in EC:EMC:MP show lower, almost identical numbers of FI. The numbers of NTI and PTI are for all electrolytes negligibly small (see SI Fig. S21).

Impact on the transport parameters.—Having identified the viscosity, the diffusion mechanism and the formation of ion

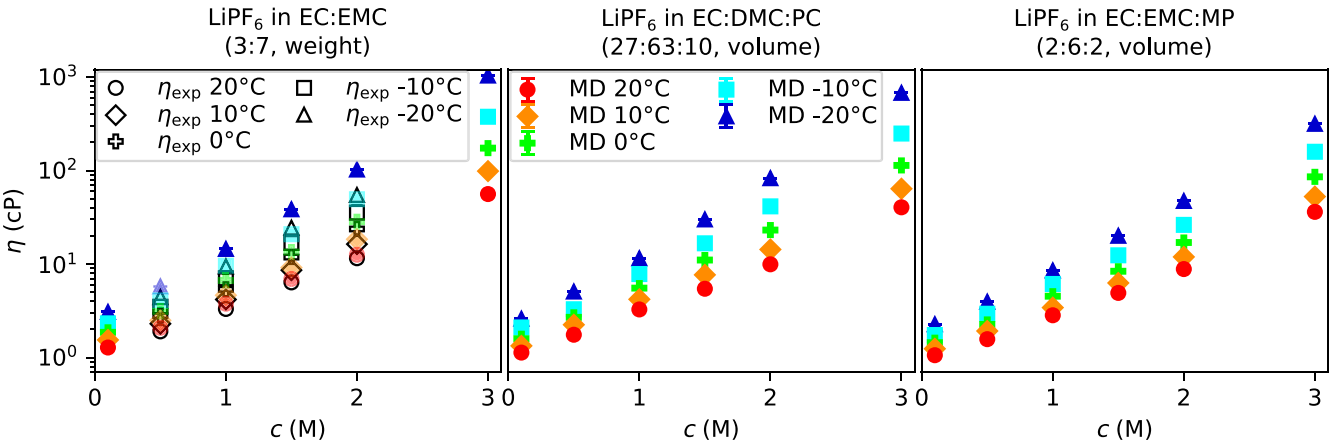

Figure 5. Calculated viscosity η using MD simulations. The experimental data points η_{exp} correspond to the Arrhenius fits of the experimental values from Logan et al.[24] (see SI Fig. S13a).

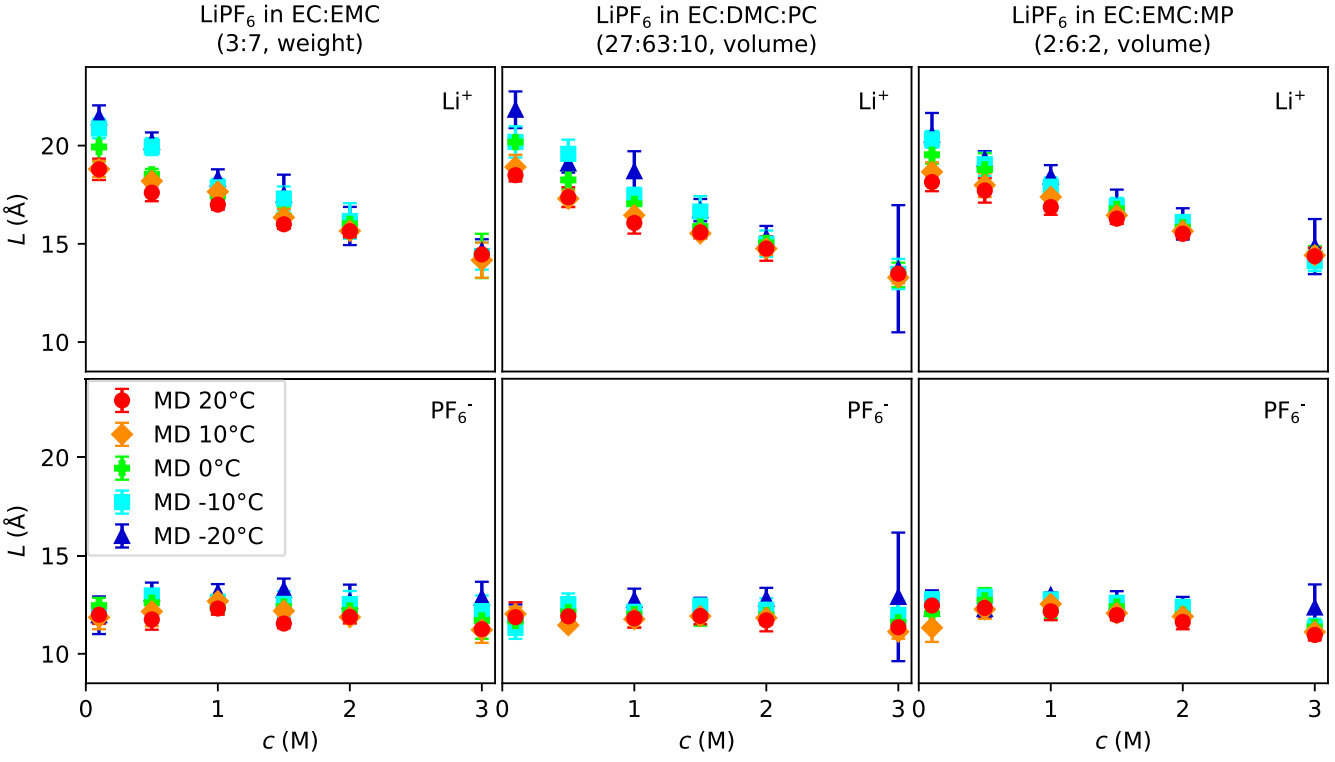

Figure 6. Composition-weighted diffusion length L of the solvent molecules, surrounding the Li^+ and the PF_6^- ions.

associations for our three electrolytes, we now estimate their impact on the conductivity, the transference number and the diffusion coefficient. The conductivity of an electrolyte depends on the concentration, the association and the mobility of the ions. Electrolytes containing highly mobile and charged ions reveal increased conductivity values. Here, we choose the free ions (FI, see Fig. 7) as a descriptor to analyze the impact of ion concentration and ion association on the ion conductivity. Additionally, we calculate the electrophoretic mobilities (see SI Fig. S22), depending on the prevalent diffusion mechanism of the ions and especially on the viscosity η (see SI Section S1.12).

The combination of the monotonic electrophoretic mobilities and the FI concentrations leads to the conductivities shown in Fig. 1. At low salt concentrations, high mobilities are countered by low FI concentrations, resulting in reduced conductivities. At intermediate concentrations, both quantities are sufficiently large to allow for maximum conductivities before they simultaneously decrease at elevated salt concentrations. The temperature dependencies of the mobilities and the FI concentrations are opposite: While the mobilities increase with temperature, the FI concentrations decrease. However, the impact of the mobilities on the conductivity seems to dominate the impact of the FI concentrations for our electrolytes, as we observe increasing conductivity trends with temperature.

$LiPF_6$ in EC:DMC:PC exhibits the highest electrophoretic mobilities and FI concentrations, and therefore it takes the overall highest conductivity values. On the other hand, $LiPF_6$ in EC:EMC:MP shows lower mobilities and FI concentrations that leads to slightly decreased conductivities. Nevertheless, due to the less prominent decrease of the mobilities with decreasing temperature, $LiPF_6$ in EC:EMC:MP surpasses the conductivity in EC:DMC:PC at -20 °C. Finally, since $LiPF_6$ in EC:EMC contains similar FI concentrations to those in EC:EMC:MP but simultaneously exhibits

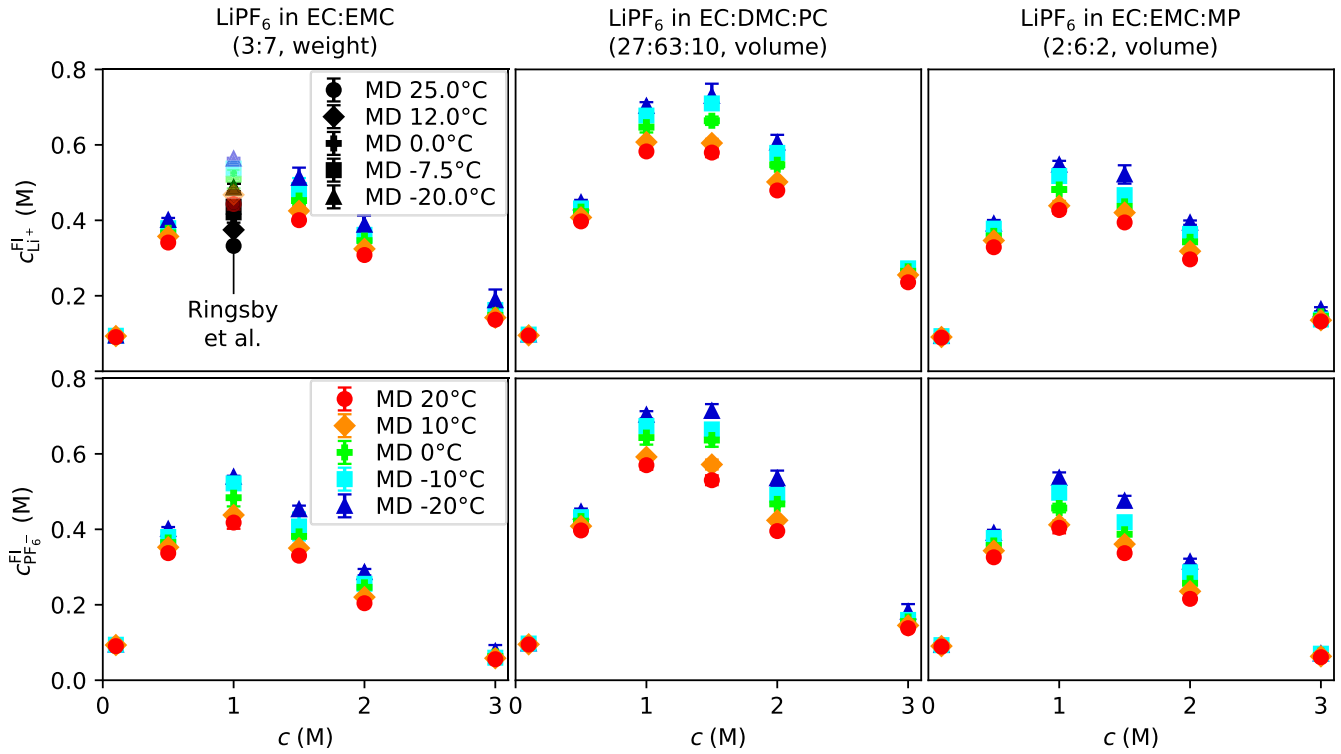

Figure 7. Concentrations of free Li^+ and PF_6^- ions calculated by MD simulations. For 1 M $LiPF_6$ in EC:EMC, our FI concentrations match the data from Ringsby et al.,[16] using a scaling factor of $\zeta = 0.8$ in their MD simulations.

the lowest electrophoretic mobilities, it becomes the least conductive of this study.

The transference number t_+^{COM} depends on differences in the formation of ion associations and the corresponding electrophoretic mobilities of anions and cations. Faster electrophoretic Li^+ ion mobilities and elevated free Li^+ concentrations lead to increased values of t_+^{COM}. As evident in Fig. 6, the Li^+ ions show decreasing diffusion lengths L with increasing salt concentration for all three electrolytes, indicating a transition from vehicular to a more structural type of diffusion mechanism. Additionally, using again the FI concentrations to estimate the impact of ion association on t_+^{COM} reveals elevated FI concentrations of lithium cations compared to the PF_6^- ions (see Fig. 7). This suggests that more anions participate in larger ion associations. Combining both results leads to a slight increase of t_+^{COM} with increasing concentration and even to $t_+^{COM} \approx t_-^{COM}$ at $c = 3.0$ M (see SI Fig. S3). The PF_6^- ions exhibit a diffusion process that is overall more structural, which explains the low transference numbers for $c < 3.0$ M.

The diffusion coefficient $D_\pm^{COM}$ follows similar dependencies as the conductivity. According to the Einstein-Smoluchowski relation, the diffusion coefficient for dilute electrolytes (electrolytes without ion-ion correlations) is directly proportional to the electrophoretic mobility. Therefore, elevated mobilities result in faster diffusion processes. As mentioned above, the mobilities depend on the prevalent diffusion mechanism and more prominently on the viscosity. Since the viscosity increases with concentration and decreases with temperature, $D_\pm^{COM}$ is expected to exhibit contrary trends. However, while the diffusion coefficient in fact increases with temperature, it still shows elevated values at high concentrations. This is due to the fact that TDF^{COM} increases with concentration and therefore compensates the loss in mobility (see SI Fig. S3). Interestingly, TDF^{COM} has the highest value for the electrolyte with the lowest viscosity, and vice versa. Therefore, the diffusion coefficients are similar for all three systems.

Conclusion

In this work, we combined MD simulations with measurements on conductivity and concentration cells in order to determine the electrolyte parameters of $LiPF_6$ in solutions of EC:EMC (3:7, weight), EC:DMC:PC (27:63:10, volume), and EC:EMC:MP (2:6:2, volume) at $-20\,°C \leqslant T \leqslant 20\,°C$ and $0.1\,M \leqslant c \leqslant 3.0\,M$. In contrast to commonly used polarization experiments, our method avoids the error-prone usage of Li metal electrodes with carbonate-based electrolytes.

For the MD simulations, we employed the non-polarizable OPLS force fields with a constant scaling factor ζ, reducing the effective charges of the involved Li^+ and PF_6^- ions. To calibrate ζ, we compared the simulated conductivities to experimental data. This allows for a more precise determination of the transference number t_+. The combination of the simulated transference number with experimental data from concentration cells enabled the deconvolution of the thermodynamic factor TDF and the calculation of the diffusion coefficient $D_\pm$. For the purpose of validating our MD simulations, we employed eNMR measurements and determined t_+ for $LiPF_6$ in EC:EMC and in EC:EMC:MP. For both electrolytes, the experimental data show strong agreement with the calculations. However, comparing our data to the electrolyte parameters determined by polarization experiments using Li metal electrodes yielded significant deviations, especially for the salt diffusion coefficient $D_\pm$. These discrepancies can be attributed to detrimental interphasial effects between the Li metal electrodes and the carbonate-based electrolytes, which make the evaluation of the polarization experiments unfeasible.[6,8,9]

Additionally, we evaluated the electrolyte viscosity, the diffusion mechanisms, and the formation of ion associations and qualitatively estimated their impact on the individual transport parameters.

Acknowledgments

We gratefully acknowledge the support by the project DeepBat, a collaboration between the National Aeronautics and Space

Administration - Jet Propulsion Laboratory (NASA - JPL) and the German Aerospace Center (DLR), and appreciate the support by the state of Baden-Württemberg through bwHPC and the German Research Foundation (DFG) through grant no INST 40/575-1 FUGG (JUSTUS 2 cluster). We acknowledge funding of the NMR spectrometer by the DFG (German Science Foundation) via project ID 452849940. We express our gratitude to the Center for Electrochemical Energy Storage Ulm & Karlsruhe (CELEST) and gratefully acknowledge the glass-blowing of the University of Stuttgart for manufacturing the concentration cells. We thank Prof. Dr. Kara Fong and Alexandra Ringsby for their helpful and inspiring correspondence and are grateful to Prof. Dr. Agilio Padua for providing the fftool on Github, which facilitated the preparation of the input files for the MD simulations. Lukas Lehnert contributed to the conceptualization of the paper, wrote the text and created the Figs. of the manuscript and the supplementary information. He mixed the examined electrolytes and performed the concentration cell measurements, implemented and parametrized the MD simulations and analyzed and interpreted the obtained data. Martin Lorenz and Prof. Dr. Monika Schönhoff performed and analyzed the eNMR data of the electrolytes and wrote the corresponding theory and experimental sections. Dr. Maria Fernanda Juarez supervised the MD simulations and reviewed the whole article. Dr. Max Schammer and Dr. Maryam Nojabaee supervised and reviewed the employed continuum electrolyte theory and the concentration cell measurements, respectively. Prof. Dr. Birger Horstmann supervised the whole work, contributed to the conceptualization of the paper, reviewed the article, and acquired the funding. The authors declare no conflict of interest.

ORCID

Lukas Lehnert https://orcid.org/0009-0008-1630-3168
Maria Fernanda Juarez https://orcid.org/0000-0002-6757-8136
Max Schammer https://orcid.org/0000-0002-9598-8343
Maryam Nojabaee https://orcid.org/0000-0001-5225-3526
Monika Schönhoff https://orcid.org/0000-0002-5299-783X
Birger Horstmann https://orcid.org/0000-0002-1500-0578

References

1. A. Latz and J. Zausch, *Journal of Power Sources*, **196**, 3296 (2011).
2. A. Latz and J. Zausch, *Beilstein Journal of Nanotechnology*, **6**, 987 (2015).
3. M. Schammer, B. Horstmann, and A. Latz, *J. Electrochem. Soc.*, **168**, 026511 (2021).
4. J. Landesfeind and H. A. Gasteiger, *J. Electrochem. Soc.*, **166**, A3079 (2019).
5. A. Nyman, M. Behm, and G. Lindbergh, *Electrochimica Acta*, **53**, 6356 (2008).
6. H. K. Bergstrom, K. D. Fong, and B. D. McCloskey, *J. Electrochem. Soc.*, **168**, 060543 (2021).
7. L. O. Valøen and J. N. Reimers, *J. Electrochem. Soc.*, **152**, A882 (2005).
8. L. Lehnert, M. Nojabaee, A. Latz, and B. Horstmann, *ChemElectroChem*, **11** (2024).
9. S. D. Talian, J. Bobnar, A. R. Sinigoj, I. Humar, and M. Gaberšček, *The Journal of Physical Chemistry C*, **123**, 27997 (2019).
10. M. Gouverneur, F. Schmidt, and M. Schönhoff, *Phys. Chem. Chem. Phys.*, **20**, 7470 (2018).
11. M. Brinkkötter, G. A. Giffin, A. Moretti, S. Jeong, S. Passerini, and M. Schönhoff, *Chem. Commun.*, **54**, 4278 (2018).
12. M. Gouverneur, J. Kopp, L. van Wüllen, and M. Schönhoff, *Phys. Chem. Chem. Phys.*, **17**, 30680 (2015).
13. Z. Zhang and L. A. Madsen, *The Journal of Chemical Physics*, **140**(8), 084204 (2014).
14. K. D. Fong, H. K. Bergstrom, B. D. McCloskey, and K. K. Mandadapu, *AIChE J.*, **66**, e17091 (2020).
15. K. D. Fong, J. Self, B. D. McCloskey, and K. A. Persson, *Macromolecules*, **53**, 9503 (2020).
16. A. J. Ringsby, K. D. Fong, J. Self, H. K. Bergstrom, B. D. McCloskey, and K. A. Persson, *J. Electrochem. Soc.*, **168**, 080501 (2021).
17. C. Fang, D. M. Halat, A. Mistry, J. A. Reimer, N. P. Balsara, and R. Wang, *Chemical Science*, **14**, 5332 (2023).
18. Y. Shim, *Phys. Chem. Chem. Phys.*, **20**, 28649 (2018).
19. A. Mistry, Z. Yu, L. Cheng, and V. Srinivasan, *J. Electrochem. Soc.*, **170**, 110536 (2023).
20. R. Kubo, *Rep. Prog. Phys.*, **29**, 255 (1966).
21. V. Chaban, *Phys. Chem. Chem. Phys.*, **13**, 16055 (2011).
22. B. Doherty, X. Zhong, S. Gathiaka, B. Li, and O. Acevedo, *Journal of Chemical Theory and Computation*, **13**, 6131 (2017).
23. D. Bedrov, J.-P. Piquemal, O. Borodin, A. D. MacKerell, B. Roux, and C. Schröder, *Chem. Rev.*, **119**, 7940 (2019).
24. E. R. Logan, E. M. Tonita, K. L. Gering, and J. R. Dahn, *J. Electrochem. Soc.*, **165**, A3350 (2018).
25. T. T. D. Nguyen, S. Abada, A. Lecocq, J. Bernard, M. Petit, G. Marlair, S. Grugeon, and S. Laruelle, *World Electric Vehicle Journal*, **10**, 79 (2019).
26. M. C. Smart, B. V. Ratnakumar, R. C. Ewell, S. Surampudi, F. J. Puglia, and R. Gitzendanner, *Electrochimica Acta*, **268**, 27 (2018).
27. M. C. Smart, B. V. Ratnakumar, L. D. Whitcanack, K. A. Smith, S. Santee, R. Gitzendanner, and V. Yevoli, *ECS Trans.*, **11**, 99 (2008).
28. M. C. Smart, B. V. Ratnakumar, K. B. Chin, and L. D. Whitcanack, *J. Electrochem. Soc.*, **157**, A1361 (2010).
29. J. L. Banks et al., *Journal of Computational Chemistry*, **26**, 1752 (2005).
30. K. D. Fong, (2022), PhD Thesis(University of California, Berkeley).
31. L. Onsager, *Phys. Rev.*, **37**, 405 (1931).
32. L. Onsager, *Phys. Rev.*, **38**, 2265 (1931).
33. H.-G. Steinrück et al., *Energy & Environmental Science*, **13**, 4312 (2020).
34. A. A. Wang, S. Greenbank, G. Li, D. A. Howey, and C. W. Monroe, *Cell Reports Physical Science*, **3**, 101047 (2022).
35. A. Mistry, L. S. Grundy, D. M. Halat, J. Newman, N. P. Balsara, and V. Srinivasan, *J. Electrochem. Soc.*, **169**, 040524 (2022).
36. T. Jung, A. A. Wang, and C. W. Monroe, *ACS Omega*, **8**, 21133 (2023).
37. A. Mistry, H.-G. Steinrück, M. F. Toney, N. P. Balsara, and V. Srinivasan, *The Journal of Physical Chemistry C*, **129**, 2874 (2025).
38. E. Sanz and C. Vega, *The Journal of Chemical Physics*, **126**, 014507 (2007).
39. A. S. Paluch, S. Jayaraman, J. K. Shah, and E. J. Maginn, *The Journal of Chemical Physics*, **133**, 124504 (2010).
40. J. G. Kirkwood and F. P. Buff, *The Journal of Chemical Physics*, **19**, 774 (1951).
41. N. Dawass, P. Krüger, S. K. Schnell, J.-M. Simon, and T. Vlugt, *Fluid Phase Equilibria*, **486**, 21 (2019).
42. B. Cheng, *The Journal of Chemical Physics*, **157**, 121101 (2022).
43. J. S. Newman, *Electrochemical Systems* (J. Wiley) (2004).
44. A. P. Thompson et al., *Comput. Phys. Commun.*, **271**, 108171 (2022).
45. (2021), Schrödinger Release 2021-1:Maestro, Schrödinger, LLC, New York, NY.
46. K. P. Jensen and W. L. Jorgensen, *Journal of Chemical Theory and Computation*, **2**, 1499 (2006).
47. J. N. Canongia Lopes and A. A. H. Pádua, *The Journal of Physical Chemistry B*, **108**, 16893 (2004).
48. L. Martìnez, R. Andrade, E. G. Birgin, and J. M. Martìnez, *Journal of Computational Chemistry*, **30**, 2157 (2009).
49. S. Nosé, *Mol. Phys.*, **52**, 255 (1984).
50. S. Nosé, *The Journal of Chemical Physics*, **81**, 511 (1984).
51. W. G. Hoover, *Phys. Rev. A*, **31**, 1695 (1985).
52. W. G. Hoover, *Phys. Rev. A*, **34**, 2499 (1986).
53. W. C. Swope, H. C. Andersen, P. H. Berens, and K. R. Wilson, *The Journal of Chemical Physics*, **76**, 637 (1982).
54. R. W. Hockney, *Computer Simulation using Particles* (A. Hilger) (1989).
55. K. D. Fong, https://github.com/kdfong/transport-coefficients-MSD.
56. N. Michaud-Agrawal, E. J. Denning, T. B. Woolf, and O. Beckstein, *Journal of Computational Chemistry*, **32**, 2319 (2011).
57. R. J. Gowers et al., "MDAnalysis: a Python package for the rapid analysis of molecular dynamics simulations." *Proceedings of the 15th Python in Science Conference*, 105 (2016).
58. Sigma-Aldrich® https://www.sigmaaldrich.com.
59. M. H. Kowsari, S. Alavi, B. Najafi, K. Gholizadeh, E. Dehghanpisheh, and F. Ranjbar, *Phys. Chem. Chem. Phys.*, **13**, 8826 (2011).
60. A. Savitzky and M. J. E. Golay, *Anal. Chem.*, **36**, 1627 (1964).
61. D. S. Hall, J. Self, and J. R. Dahn, *The Journal of Physical Chemistry C*, **119**, 22322 (2015).
62. R. Naejus, D. Lemordant, R. Coudert, and P. Willmann, *The Journal of Chemical Thermodynamics*, **29**, 1503 (1997).
63. M. Schammer, "Transport theory for highly correlated electrolytes with non-local species interactions." (2023), Ph.D. thesis.
64. M. Lorenz, F. Kilchert, P. Nürnberg, M. Schammer, A. Latz, B. Horstmann, and M. Schönhoff, *The Journal of Physical Chemistry Letters*, **13**, 8761 (2022).
65. F. Kilchert, M. Lorenz, M. Schammer, P. Nürnberg, M. Schönhoff, A. Latz, and B. Horstmann, *Phys. Chem. Chem. Phys.*, **25**, 25965 (2023).
66. H. Lundgren, M. Behm, and G. Lindbergh, *J. Electrochem. Soc.*, **162**, A413 (2014).
67. C. L. Berhaut, P. Porion, L. Timperman, G. Schmidt, D. Lemordant, and M. Anouti, *Electrochimica Acta*, **180**, 778 (2015).
68. F. Schmidt, A. Pugliese, C. C. Santini, F. Castiglione, and M. Schönhoff, *Magnetic Resonance in Chemistry*, **58**, 271 (2020).
69. M. Holz, *Chem. Soc. Rev.*, **23**, 165 (1994).
70. E. Pettersson, I. Furó, and P. Stilbs, *Concepts in Magnetic Resonance Part A*, **22A**, 61 (2004).
71. G. C. Sosso, J. Chen, S. J. Cox, M. Fitzner, P. Pedevilla, A. Zen, and A. Michaelides, *Chem. Rev.*, **116**, 7078 (2016).
72. E. R. Logan, K. L. Gering, X. Ma, and J. Dahn, *The Electrochemical Society Interface*, **28**, 49 (2019).
73. K. L. Gering, *Electrochimica Acta*, **51**, 3125 (2006).
74. K. L. Gering, *Electrochimica Acta*, **225**, 175 (2017).
75. K. W. Gao and N. P. Balsara, *Solid State Ionics*, **364**, 115609 (2021).
76. J.-P. Hansen and I. R. McDonald, *Theory of Simple Liquids* (Elsevier Science & Technology Books) (1990).

77. M. H. C. Peiris, S. Brennan, D. Liepinya, H. Liu, and M. Smeu, *Colloids and Surfaces A: Physicochemical and Engineering Aspects*, **674**, 131831 (2023).
78. J. Self, K. D. Fong, and K. A. Persson, *ACS Energy Lett.*, **4**, 2843 (2019).
79. S. Han, *Sci. Rep.*, **7**, 46718 (2017).
80. A. von Cresce and K. Xu, *Electrochem. Solid-State Lett.*, **14**, A154 (2011).
81. K. Xu and A. von Wald Cresce, *J. Mater. Res.*, **27**, 2327 (2012).
82. K. Xu, Y. Lam, S. S. Zhang, T. R. Jow, and T. B. Curtis, *The Journal of Physical Chemistry C*, **111**, 7411 (2007).
83. D. M. Seo, S. Reininger, M. Kutcher, K. Redmond, W. B. Euler, and B. L. Lucht, *The Journal of Physical Chemistry C*, **119**, 14038 (2015).
84. M. T. Ong, O. Verners, E. W. Draeger, A. C. T. van Duin, V. Lordi, and J. E. Pask, *The Journal of Physical Chemistry B*, **119**, 1535 (2015).
85. O. Borodin, M. Olguin, P. Ganesh, P. R. C. Kent, J. L. Allen, and W. A. Henderson, *Phys. Chem. Chem. Phys.*, **18**, 164 (2016).
86. N. Yao et al., *Angew. Chem. Int. Ed.*, **62**, e202305331 (2023).
87. L. Yang, A. Xiao, and B. L. Lucht, *Journal of Molecular Liquids*, **154**, 131 (2010).
88. C. Berhaut, D. Lemordant, P. Porion, L. Timperman, G. Schmidt, and M. Anouti, *RSC Adv.*, **9**, 4599 (2019).
89. K. D. Fong, J. Self, K. M. Diederichsen, B. M. Wood, B. D. McCloskey, and K. A. Persson, *ACS Central Science*, **5**, 1250 (2019).
90. C. J. F. Solano, S. Jeremias, E. Paillard, D. Beljonne, and R. Lazzaroni, *The Journal of Chemical Physics*, **139**, 034502 (2013).
91. T. P. Liyana-Arachchi, J. B. Haskins, C. M. Burke, K. M. Diederichsen, B. D. McCloskey, and J. W. Lawson, *The Journal of Physical Chemistry B*, **122**, 8548 (2018).
92. M. Forsyth, H. Yoon, F. Chen, H. Zhu, D. R. MacFarlane, M. Armand, and P. C. Howlett, *The Journal of Physical Chemistry C*, **120**, 4276 (2016).
93. D. Orbakh, *Nonaqueous Electrochemistry* (Marcel Dekker) (1999).
94. R. Nagl, Z. Fan, C. Nobis, C. Kiefer, A. Fischer, T. Zhang, T. Zeiner, and M. Fischlschweiger, *Journal of Molecular Liquids*, **386**, 122449 (2023).
95. B. P. Kar, N. Ramanathan, K. Sundararajan, and K. Viswanathan, *Journal of Molecular Structure*, **1072**, 61 (2014).
96. H. Lee, S. Hwang, M. Kim, K. Kwak, J. Lee, Y.-K. Han, and H. Lee, *The Journal of Physical Chemistry Letters*, **11**, 10382 (2020).
97. M. S. Ding, K. Xu, S. S. Zhang, K. Amine, G. L. Henriksen, and T. R. Jow, *J. Electrochem. Soc.*, **148**, A1196 (2001).
98. N. Bjerrum, *Det Kgl. Danske Videnskabernes Selskab* (1926).
99. Y. Marcus and G. Hefter, *Chem. Rev.*, **106**, 4585 (2006).
100. G. G. Stokes et al., *Pitt Press Cambridge* (1851).
101. S. H. Jamali, R. Hartkamp, C. Bardas, J. Söhl, T. J. H. Vlugt, and O. A. Moultos, *Journal of Chemical Theory and Computation*, **14**, 5959 (2018).
102. M. Schoen and C. Hoheisel, *Mol. Phys.*, **56**, 653 (1985).
103. B. Hess, *The Journal of Chemical Physics*, **116**, 209 (2002).
104. Y. Zhang and E. J. Maginn, *The Journal of Physical Chemistry B*, **125**, 13246 (2021).